PCCP

Accepted Manuscript

ROYAL SOCIETY OF CHEMISTRY

www.rsc.org/pccp

Journal Name
ARTICLE

The Thermoelectrochemistry of Lithium-Glyme Solvate Ionic Liquids: Towards Waste Heat Harvesting

Jeffrey J. Black,[a] Thomas Murphy,[b] Rob Atkin,[b] Andrew Dolan[a] and Leigh Aldous[a,*]

Received 00th January 20xx,
Accepted 00th January 20xx

DOI: 10.1039/x0xx00000x

www.rsc.org/

Thermoelectrochemistry offers a simple, scalable technique for direct conversion of waste heat into useful electricity. Here the thermoelectrochemical properties of lithium-glyme solvate ionic liquids, as well as their dilute electrolyte analogues, have been investigated using mixtures of tetraglyme (G4, tetraethylene glycol dimethyl ether) and lithium bis(trifluoromethylsulfonyl)imide (Li[NTf_2]). The thermoelectrochemical process is entropically-driven by release of the glyme from the lithium-glyme complex cation, due to electrodeposition of lithium metal at the hotter lithium electrode with concomitant electrodissolution at the cooler lithium electrode. The optimum ratio for thermochemical electricity genaration is not the solvate ionic liquid (equimolar mixture of Li[NTf_2] and glyme), but rather one Li[NTf_2] to four G4, due to the mixtures relatively high ionic conductivity and good apparent Seebeck coefficient (+1.4 mV K^{-1}). Determination of the lithium-glyme mixture thermal conductivity enabled full assessment of the Figure of Merit (ZT), and the efficiency relative to the Carnot efficiency to be determined. As the lithium electrodeposits are porous, alternating the temperature gradient results in a system that actually improves with repeated use.

Introduction

Across the globe electricity is produced from heat in various ways on an industrial scale. Many of these methods require multiple processes and numerous moving parts to function. However, vast quantities of heat also go to waste in these processes. Waste heat is also generated by combustion engines, solar panels, *etc*.[1] A living human body typically radiates waste heat into its surroundings, continuously dissipating *ca.* 100 Watts of thermal energy.[2] New options to efficiently and economically harvest and utilise this wasted energy are highly desirable.

The Seebeck effect is arguably the simplest method available for waste heat utilisation, as a thermal gradient is converted directly into electrical energy without moving parts.[1] This effect can be harnessed by solid-state semi-conductors (thermoelectric devices), which rely upon hole-electron conduction, or by redox-based systems (thermoelectrochemical or thermogalvanic devices).

The majority of thermoelectric systems used today rely on expensive and fragile semiconductor components that typically contain rare metalloids such as Bi_2Te_3.[3] Other materials used in thermoelectric devices are antimony-doped skudderites,[4] zintl phases,[5] or complex nanofabricated BiTe alloys.[6] These devices suffer from low efficiencies, high costs and are prone to breakage from impacts such as drops, large thermal gradients or thermal cycling,[7] the latter of which can raise serious questions about their use in generating electricity from variable thermal gradients.

Thermoelectrochemical cells composed of a liquid or solid-state electrolyte and a suitable redox active species can overcome some of the problems associated with semiconductor-based devices. For example, they can be flexible, allowing them to conform to irregular shapes.[2, 7] The redox couples used can also be quite cheap and made from abundant materials, as well as being suited to harvesting low-grade waste heat.[8-10] They are also eminently scalable; while performance is significantly affected by changes in electrode separation,[11] the geometric area of parallel electrodes can be readily expanded with corresponding boosts in power. Nanostructuring the electrodes can further boost both power and efficiency.[12, 13] Individual cells can also be connected in parallel and series to multiply the power output.[14]

The Seebeck coefficient (S_e) is a measure of the potential difference (V_{OC}, the open circuit potential) between two electrodes with a common electrolyte as a function of temperature difference between the electrodes (ΔT). It is proportional to the entropy difference between the redox states (ΔS) as shown by equation 1.[9]

$$S_e = \frac{V_{OC}}{\Delta T} = \frac{\Delta S}{nF} \qquad (1)$$

The maximum power and efficiency of thermoelectric systems are proportional to the square of the Seebeck coefficient.[15] The number of charge carriers and their

[a] School of Chemistry, UNSW Australia, Sydney, NSW 2052, Australia.
[b] Priority Research Centre for Advanced Fluids and Interfaces, Newcastle Institute for Energy and Resources, The University of Newcastle, Callaghan , NSW 2308, Australia.
† Please direct all correspondence to Leigh Aldous: l.aldous@unsw.edu.au.

Electronic Supplementary Information (ESI) available: [Included as Supplementary information is a diagram of the experimental setup, a graph showing the Seebeck values obtained, the viscosity data measured across a range of temperatures, a Walden Plot, photos and schematic of components of a cell after long term discharge, a comparison between mole ratio and other expressions of concentration and the equation for maximum theoretical efficiency of a heat engine]. See DOI: 10.1039/x0xx00000x

diffusivity are also critical in ensuring maximum power output and efficiency.[16]

Most research into thermoelectrochemical cells has been focused upon redox couples with two solvated species (*e.g.* ferro/ferricyanide) or one solvated species (*e.g.* copper(0)/copper(II)).[17] A change in ordering around the different species is the entropic driving force behind heat-to-power conversion. The majority of studies have utilized aqueous electrolytes containing inorganic redox couples. A prime example is ferri/ferrocyanide, which has a relatively large Seebeck coefficient of *ca.* -1.4 mV/K.[9, 13, 15] However water can be a major limitation due to its limited liquidus range, and its reactivity with a wide range of potential redox couples. Recently organic solvents,[18] as well as protic[8] and aprotic ionic liquids,[9, 10, 19] and solvent-ionic liquid mixtures[20] have been investigated as alternatives. However, the solubility of the redox species rarely exceeds 1 M in these liquids.[16]

Lithium ion thermogalvanic cells have been reported with electrodes consisting of lithium intercalation compounds (Li_xTiS_2 or $Li_xV_2O_5$) in contact with 1 M $Li[PF_6]$ or $Li[BF_4]$ in either propylene carbonate, or a 1:1 mixture of ethylene carbonate and dimethyl carbonate.[21] Seebeck coefficients were on the order of *ca.* +1.0 ± 0.2 mV K^{-1}.[21]

In this study, the thermoelectrochemistry of a relatively new class of 'super-concentrated' electrolytes are investigated. Glymes (or glycol diethers) are polyether oligomers with exceptional solubility for alkali metal salts in general, and lithium in particular.[22] When a suitable glyme is mixed in a 1:1 ratio with lithium salts with poorly coordinating anions,[23] a 'solvate ionic liquid' forms. These are classed as ionic liquids, as they are essentially 100% ionic in nature, and possess the high conductivity and viscosity,[24] enhanced electrochemical stability[25] and low vapour pressures[23] expected of conventional ionic liquids. Solvate ionic liquids are also redox active (all cationic complexes contain lithium), and typically possess lithium cation concentrations approaching 3 molar. Solvate ionic liquids are of particular interest for lithium-based batteries,[25, 26, 27] and their behaviour at electrode surfaces has been examined.[28]

It has been suggested that glymes wrap around lithium ions in structures reminiscent of crown ethers,[29] but recent neutron diffraction measurements[30] and molecular dynamic simulations[31] have revealed that the true situation is far more complex. Regardless of the precise 'structure' of the complex liquid and the role of the anion, it is clear from these structural studies and NMR diffusion data[29] that a lithium ion and glyme are strongly associated and it is expected that solvation of a lithium ion from an electrode surface requires a significant reorganisation of solvent (as in water) resulting in a large entropy change. While much prior research has focussed upon pure 1:1 solvate ionic liquids, for application-driven research there is no necessity that a 1:1 molar ratio of salt to glyme be maintained. Indeed, the conductivity of lithium[32] and sodium[33] salt and glyme mixtures have been found to peak at ratios lower than 1:1.

In this work the thermoelectrochemistry of lithium bis(trifluoromethylsulfonyl)imide dissolved in tetraethylene glycol dimethyl ether (or tetraglyme) was investigated, using solid lithium metal electrodes. This was prompted by an anticipation that (i) solvation and desolvation of the lithium cation by the flexible glyme molecule will lead to large entropy changes, and should therefore result in a favourable Seebeck coefficient, and (ii) the high lithium contents achievable (*ca.* 3 M) could result in high-power thermoelectrochemical devices. The electrolyte concentration was ranged from dilute through to the 'solvate ionic liquid' composition and beyond.

Experimental

Lithium bis(trifluoromethylsulfonyl)imide ($Li[NTf_2]$) was obtained from IoLiTec (Germany), tetraethylene glycol dimethyl ether (G4) was obtained from Tokyo Chemical Industry (Japan), hexane was obtained from Scharlau (Spain) and lithium discs and CR2032 battery casings were obtained from MTI Corporation (USA). All chemicals were immediately taken into an argon-filled glovebox upon receipt and, with the exception of the lithium disc, used without further purification. Lithium discs were either used as received or after cleaning (different treatments noted in the text) by scrubbing gently with a toothbrush in hexane for approximately 10 seconds on each face of the disc, following a previously reported cleaning methodology.[34]

The $Li[NTf_2]$ and G4 solutions were prepared by accurately weighing the components (salt and solvent) in an argon filled glovebox and stirring with a magnetic stirrer until fully dissolved. They will be referred to by their mole ratio (moles of $Li[NTf_2]$ per mole of G4). Table S2 displays the mole ratio values for all samples, as well as their equivalents in terms of molarity of Li^+ (valid only at 20 °C) and mole percent of $Li[NTf_2]$ in the systems.

Cells were prepared by placing a lithium disc in the 'top' half of the battery casing (smallest half), followed by a nylon washer. Nylon washers were 3D printed to create a 1.9 mm high disc with a 9 mm internal diameter cavity, which fitted into the CR2032 casing. The cell was then filled with the electrolyte solution and another lithium disc placed on top (separated from the other lithium disc by the washer). The 'bottom' of the battery casing was then placed over the top and crimped using a hydraulic crimping machine.

The cells were tested using an in house tester, shown in Figure S1 in the supplementary content, consisting of an Arduino microcontroller controlling two Peltier devices to heat/cool each side of the cell. The cold side of the cell was kept at 20 °C, and the hot side temperature was varied as required. During all measurements, the cell was kept on its side, *e.g.* as opposed to a 'hot-over-cold' arrangement.[15] All measurements were made using a Keysight B2900A SMU (TRIO Test & Measurement Pty Ltd, Australia).

The Seebeck coefficient was determined by measuring the open circuit potential for the cell for 1,000 seconds, then averaging the potential over the final 500 seconds, at temperature differences of 10, 20, 30, 40 and 50 K. The initial 500 seconds were to allow the cell to reach the target temperature and stabilise.

The power measurements were obtained by measuring the open circuit potential for 10 minutes and averaging the data

from the last 5 minutes, with the first 5 minutes used to allow the cell to stabilise. The SMU was then configured to draw current from the cell to have the voltage of the cell be 0.75, 0.5, 0.25 and 0 times the open circuit potential. The current was measured for a period of 10 minutes, averaging the last 5 minutes to obtain the current for the cell. This was divided by the area of exposed lithium to obtain the current density which was multiplied by the voltage to obtain the power density. As the cells displayed an inverse linear relationship between current and voltage the maximum power density can be determined by Equation 2.

$$PD_{max} = \frac{J_{SC}V_{OC}}{4} \quad (2)$$

Additional long term measurements were made for cells with a mole ratio of 0.22 Li[NTf_2] per G4. One form of measurement involved recording the power density curve (from open circuit potential to short circuit current density) every hour for an extended duration (*e.g.* 2 weeks), in order to monitor the potential, current and power from the cell when exposed to a constant temperature gradient. Another form of measurement involved continually short-circuiting the cell under a constant temperature gradient, and measuring the short circuit current density for an extended duration. Gaps in the data in the relevant figures represent when measurement was periodically ceased in order to see if the current or voltage values would recover.

Alternating temperature gradient experiments involved holding one side at 20 °C and the other at 50 °C for 2 hours, then inverting the temperature difference, alternating every 2 hours. The diameter of the nylon washer was increased to 12 mm to provide additional space for lithium metal expansion.

Density and Viscosity measurements were obtained using an Anton Paar DMA 4100 M Density Meter with a Lovis 2000 ME Microviscometer module attached (MEP Instruments, Australia). This utilizes a variable angle falling ball method, using a 1.5 mm diameter stainless steel ball in either a 1.59 mm ID glass tube for low viscosity samples, or 1.8 mm ID glass tube for high viscosity samples.

Conductivity was measured using eDAQ Pod-Vu conductivity isopod with platinum electrodes (eDAQ Pty Ltd, Australia).

Thermal conductivity, λ, was measured using a KD2 Pro Thermal Properties Analyzer (Decagon Devices Inc., US). The measurement is based on the transient hot-wire method (THW) and uses a single needle sensor (1.3 mm diameter and 60 mm long) containing both a heating element and a thermal resistor. The sensor applies a small heat pulse to the sample and simultaneously monitors temperature variations in the sample. The Thermal conductivity is calculated from a heating, and subsequent cooling, cycle using a modified version of the Carslaw and Jaeger model for an infinite line heat source[35] (from more details on the measurement see reference[36]). The needle was inserted vertically into the sample to minimize free convection induced by thermal gradients. During measurements the samples were suspended in a thermostatic water bath (Cole Palmer, Australia) set to the desired temperature, equilibrating the samples for 15 minutes prior to each measurement. The KD2 sensor, using a platinum resistance probe, also recorded the sample temperature at the time of measurement.

Results and Discussion

Thermoelectrochemical measurements

Prior studies measuring the Seebeck coefficient have typically used a U-tube setup[9] open to the atmosphere or a large cylindrical cell.[7, 18] These contain large volumes and require long time periods to equilibrate. Recent reports have detailed hermetically-sealed CR2032 battery casings.[12, 19, 37, 38] These are ideal to house reactive and volatile material, and also for 'real world' waste-heat harvesting applications by virtue of their large cross sectional area, short electrode separation and low electrolyte volume.

The temperature of the metal sample holder was precisely controlled, but a slight temperature gradient exists between these heated/cooled surfaces and the metal of the CR2032 battery casing, mainly due to the small air gap between the metal surfaces. Therefore the applied ΔT is not the real ΔT inside the casing. Aqueous systems[12, 37] and ionic liquid systems[19] in CR2032 casings have consistently given apparent Seebeck coefficient *ca.* 20% lower than the 'real' Seebeck coefficient. However, rather than correct based upon assumptions, all reported Seebeck coefficients, voltages, currents and powers are reported uncorrected, as this represents the real performance of the investigated (CR2032-based) systems

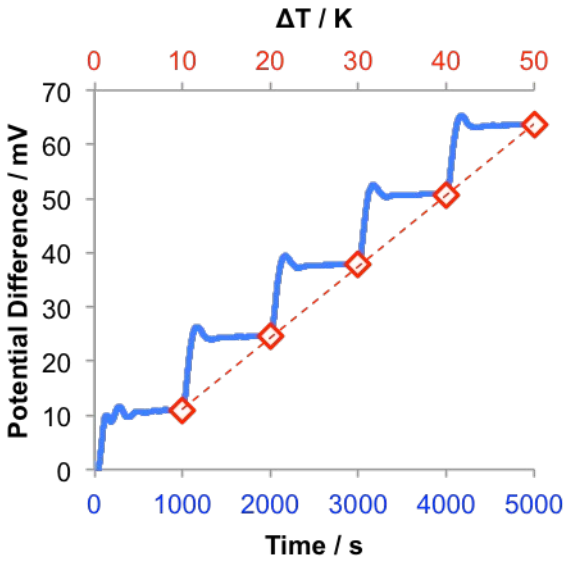

Figure 1. Raw Open Circuit Potential measurements of ~0.22 LiNTf2:G4 cell (solid blue line), showing the steps as the temperature was increased by +10 K every 1,000 s, and producing the expected linear trend for potential *vs* temperature difference.

The Seebeck coefficient was measured for Li(cooler) | Li[NTf_2], G4 | Li(hotter) assemblies as a function of the Li[NTf_2] : G4 ratio. All systems investigated (from Li[NTf_2] : G4 ratios of 0.02 Li[NTf_2] to 1.1 Li[NTf_2]) displayed clear and consistent increases in the cell open circuit potential as a function of temperature difference. Example data is shown in Figure 1, with the system quickly equilibrating and producing the expected linear trend for $\Delta E/\Delta T$ to yield the Seebeck coefficient; in this case +1.36 mV K^{-1}.

Linearity and stability was observed for individual cells (as long as current was not drawn), resulting in Seebeck coefficients with very small error. However, multiple cells containing the same solution displayed *ca.* 10% variation in the Seebeck coefficient. This is attributed to minor variations in the thermal interface between the Li metal and the steel interior of the battery casing.

Figure S2 displays the trend in Seebeck coefficient as a function of the Li[NTf_2] : G4 ratio. As the Li[NTf_2] content increased the Seebeck coefficient dropped from +1.4 ± 0.1 mV K^{-1} down to *ca.* +0.9 mV K^{-1}. In thermoelectrochemical cells, increasing the concentration of the redox species typically decreases the Seebeck coefficient, due to decreases in the redox species chemical activity coefficients in line with Debye–Hückel theory.[10, 18] An additional consideration in this study is a possible decrease in the degree of coordination between Li^+ and G4 as the Li[NTf_2] content increases. Dilute solutions of lithium salts in ethereal solvents are typically composed of solvent-separated ions, with coordination numbers of 4 to 6 for the Li^+.[39] However, recent investigation has demonstrated that in 1:1 Li[NTf_2]:G4 'solvate ionic liquids', contact ion pairs dominate; on average only *ca.* 2.27 of the 5 oxygens in G4 coordinate to Li^+, with a further 1.73 oxygens coming from $[NTf_2]^-$.[30] At present we are unable to distinguish between the relative effects of speciation *vs* thermodynamic influences, but both are interrelated and therefore influential.

Notably, as the system transitioned to the 1:1 Li[NTf_2]:G4 'solvate ionic liquid'[24, 25] and eventually an excess of Li[NTf_2], the Seebeck coefficient recovered from *ca.* +0.9 mV K^{-1} to *ca.* +1.2 mV K^{-1}. Crystal structures and spectroscopic studies of G4 in the presence of excess Li^+ has demonstrated the formation of complex assemblies with G4 binding to multiple Li^+.[39] Since this additional binding would result in the G4 being more extensively coordinated, this additional entropy change upon Li^+ reduction could account for the increase in Seebeck coefficient in this 'ionic liquid' region. Cluster analysis has identified *ca.* 10-20 % of 1:1 Li[NTf_2]:G4 is present as $[Li_2(G4)]^{2+}$.[30] Conversely, an increase in the activity coefficient of the Li^+ cannot be ruled out. The very high viscosities of these concentrated solutions prevented investigation beyond the 1.1:1 ratio.

The ferri/ferrocyanide system is arguably one of the most extensively employed aqueous thermoelectrochemical electrolytes, due to its high Seebeck coefficient of *ca.* -1.4 mV K^{-1}.[13, 15] This is driven by the extensive structuring of several water molecules around the $[ferricyanide]^{4-}$ anion. The highest Seebeck coefficient observed in this study on the Li[NTf_2]/G4 system was +1.4 ± 0.1 mV K^{-1}, indicating that Li[NTf_2]/G4 has favourable thermodynamics for thermoelectrochemical applications, due to a significant entropy change.

Thermodynamic cycles have allowed the determination of the Seebeck coefficient for the process $Li^+_{(solvated)} + e^- \Rightarrow Li_{(s)}$ in solvents which are not compatible with lithium metal.[40] The Seebeck coefficient for the process $Li^+_{(g)} + e^- \Rightarrow Li_{(s)}$ (*e.g.* determined from S° values, in the absence of a solvent) is -1.08 mV K^{-1}. Aqueous systems have strong H_2O-H_2O interactions *and* strong H_2O-Li^+ interactions; the Seebeck coefficient in aqueous systems is therefore -0.51 mV K^{-1}, and the entropic driving force is an ordered solid becoming a more disordered solution (*i.e.* the hot lithium electrode would dissolve as the anode). For ethanol, the Seebeck coefficient is +0.54 mV K^{-1}. The positive sign indicates the thermoelectrochemistry is inverted and the entropic driving force is now release of the strongly bound ethanol molecules from the Li^+ hydration sphere, to result in a more disordered solution (*i.e.* the cold lithium electrode would dissolve as the anode). The large positive Seebeck coefficient observed in this work for the G4 system (*ca.* +1.4 ± 0.1 mV K^{-1}) indicates that the entropic driving force is the release of the G4 molecule from the Li^+ solvation sphere, and during continuous discharge the lithium metal would migrate from the cooler electrode (anode) to the hotter electrode (anode).

The Seebeck coefficient is directly correlated with the entropy change in the system. A solution with 1 M Li[NTf_2] in G4 (see Table S2 for the conversion of ratios to concentration) has an apparent Seebeck value of *ca.* +1.3 mV K^{-1}. Therefore the entropy change under 'standard conditions' (1 M solution at 298 K) for the process $[Li(G4)][NTf_2] + e^- \Rightarrow Li_{(s)} + G4$ is *ca.* +130 J K^{-1} mol^{-1}. The entropy change for lithium reduction in tetrahydrofuran (8 mM Li[PF_6]) was measured

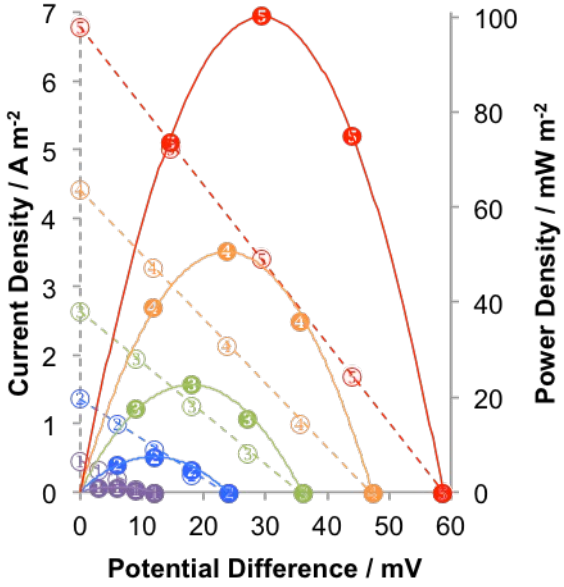

Figure 2. A plot of the power density (filled circles) and current density (empty circles) vs potential difference for an 0.22 $LiNTf_2$ per G4 cell, at temperature differences of 10, 20, 30, 40 and 50 K (❶, ❷, ❸, ❹ and ❺, respectively). Lithium electrodes were cleaned prior to use.

electrochemically and found to be +89 ± 5 J K^{-1} mol^{-1} (relative to ferrocene|ferrocenium),[41] and by microcalorimetry to be +165 ± 25 J K^{-1} mol^{-1} for 1 M Li[PF_6] in 1:1 ethylene carbonate : dimethyl carbonate.[42]

The power discharge characteristics of the various systems were also assessed by measuring voltage-current trends as a function of temperature and Li[NTf_2] : G4 ratios. Example data is shown in Figure 2 for the 0.22 Li[NTf_2] to G4 system. The system displays the anticipated linear trend between open circuit potential and temperature. The current was linearly related to the voltage, which is typical for a conventional thermoelectrochemical system (as it is a system that acts as a voltage source in series with an internal resistance), with the voltage dropping as more current was drawn from the cell. This results in a parabolic power-voltage relationship with the peak power output at half the open circuit potential. The relationship between temperature and short circuit current density is more complex; it is a combination of a linear increase in the voltage component (the Seebeck coefficient) and a non-linear increase in the current due to a near-exponential increase in the current density with increasing temperature, due to changing electron transfer constants, viscosity and conductivity (characterised and discussed later). The combined effects of increasing short circuit current densities and open circuit potentials resulted in the maximum power density increasing faster than the temperature difference squared.

Figure 3 displays a summary of the measured maximum power output at ΔT = 50 K as a function of the Li[NTf_2] : G4 ratio. Using the lithium foil discs as electrodes as received (◆) resulted in relatively stable power measurements, with a maximum power output at a ratio of approximately 0.25 Li[NTf_2] per G4. Cleaning the surfaces of the lithium foil discs prior to use (■) resulted in more uncertainty in the power measurements but also a significant (approximately order of magnitude) increase in the maximum power output of the cell, with a maximum at *ca.* 0.25 Li[NTf_2] per G4. This enhanced power output is due to removal of trace oxide from the surface of the as-received lithium foil, but the cleaning (and unavoidable roughening of the soft surface) resulted in more variation between cells. The difference in power between the surface pre-treatment steps disappeared above ratios of *ca.* 0.6; likely due to both the high viscosity and thus low conductivity, and also a lack of free glyme molecules at the anode becoming the major limiting factors (*vide infra*).

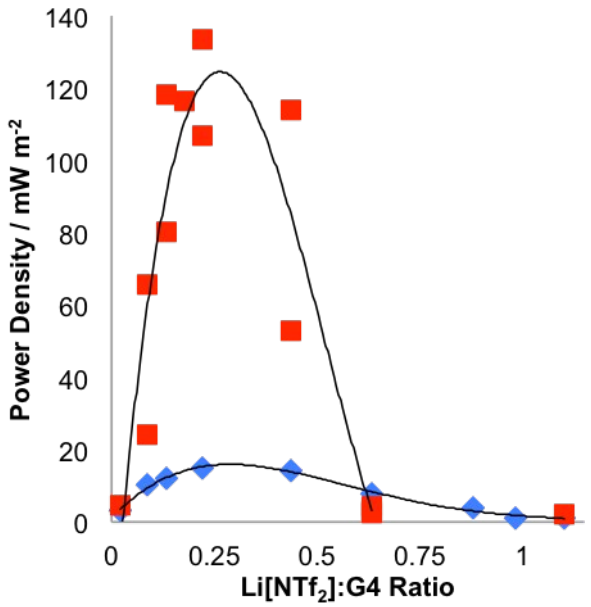

Figure 3. Maximum power at ΔT = 50 K, as a function of the Li[NTf_2] : G4 ratio, and when using as received Lithium foil discs (◆) or cleaned lithium foil discs (■).

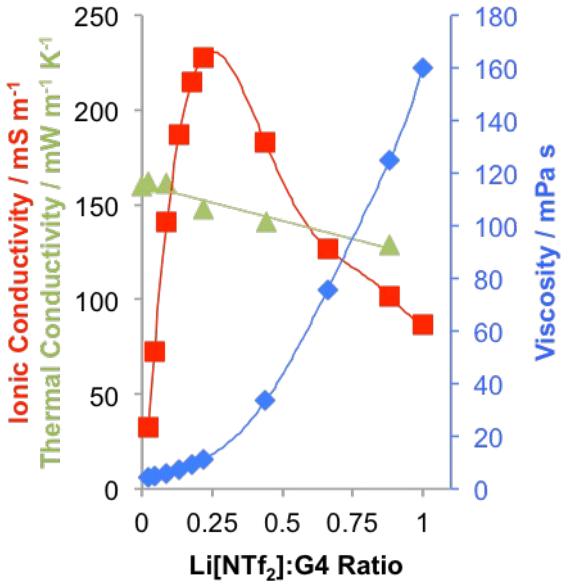

Figure 4. Mole ratio dependence on ionic conductivity (■), thermal conductivity (▲) and viscosity (◆) at 20 °C.

Characterising the physical properties of the Li[NTf_2] : G4 mixtures in relation to their thermoelectrochemistry

In order to evaluate the observed trends in thermoelectrochemical performance for the Li[NTf_2] : G4 mixtures, the viscosity, ionic conductivity and thermal conductivity were evaluated as a function of the Li[NTf_2] : G4 ratio and as a function of temperature.

As shown in Figure 4, G4 has a relatively low viscosity which rapidly increased with addition of Li[NTf_2]. Addition of Li[NTf_2] resulted in an initial increase in conductivity (to due addition of electrolyte) before the increase in viscosity became more significant than the addition of further charge carriers; as such conductivity peaked at *ca.* 0.25 Li[NTf_2] per G4. These results are in good agreement with the prior values reported by Yoshida *et al.*[32] and Zhang *et al.*[34]

Notably, the trend in conductivity in Figure 4 matches the trend in power output (*cf.* Figure 3), so the maximum power corresponds to the most conductive electrolyte. However, the conductivity decreases beyond a ratio of 0.5:1 are relatively minor, whereas the actual power above this ratio (*cf.* Figure 3) drops significantly. In this region, a lack of free glyme molecules is a possible limiting factor; in the 1:1 solvate ionic liquid composition, between 0.29% to *ca.* 5% free (uncoordinated) G4 molecules are expected.[30, 31] Furthermore,

discharging power will only further saturate the electrolyte adjacent to the anode. Lithium ion batteries are commonly tested using 'solvate ionic liquids' in the 1:1 ratio; these ratios are preferred as they enhance the electrochemical stability of the glyme, allowing higher overpotentials to be employed.[25] Notably, battery experiments typically employ large overpotentials, hence the 1:1 ratio is preferred. In thermoelectrochemical cells the overpotential is fixed and current is more easily optimised. The highest current density shown in Figure 2 (7.6 Am^{-2}) is more than an order of magnitude higher than the current densities typically employed when (dis)charging lithium batteries at moderate rates using 1:1 solutions ($^1/_8$ C, *ca.* 0.5 Am^{-2}).[25] The current density obtained in the thermoelectrochemical cells at the 1:1 ratio at ΔT = 50 K were *ca.* 0.3 ± 0.05 Am^{-2}. Different $Li[NTf_2]$: G4 ratios lead to different physicochemical properties, and clearly each application has a particular optimum ratio.

Walden plots allow the ionicity of systems to be probed.[43] Figure S4(a) displays the Walden plot for the investigated systems and shows that all ratios represent 'good' ionic systems, with slightly increasing ionicity as $Li[NTf_2]$ content increases. Also shown in Figure S4(b) is a Walden plot where the concentration of both $Li[NTf_2]$ and G4 have been factored into the molar conductivity value, resulting in two linear phases and transition phase (curved region). At lower ratios of $Li[NTf_2]$ the system is a 'dilute electrolyte' and ionicity increases rapidly. At higher ratios the system is a 'super-concentrated electrolyte' and has increasingly 'ionic liquid'-like behaviour; ionicity increases are much more incremental, and with regards to power output in this region the increases in concentration are undermined by the increase in viscosity. The curved region corresponds to an intermediate 'concentrated electrolyte' phase, with the optimum *ca.* 0.25 $Li[NTf_2]$ per G4 system found at the boundary between the concentrated and ionic liquid-like phases.

The thermal conductivity of the mixtures were also evaluated; it demonstrated a minor decrease with increasing $Li[NTf_2]$ content. The measured values (129 – 162 mW m^{-1} K^{-1}) are significantly lower than that of water (600 mW m^{-1} K^{-1}), and on par with rubber (*ca.* 170 mW m^{-1} K^{-1}) and typical ionic liquids (107 – 182 mW m^{-1} K^{-1}).[44]

The physical properties of 0.22 $LiNTf_2$ per G4 were also investigated as a function of temperature. Figure 5 demonstrates that viscosity decreases with increasing temperature, resulting in a rise in the conductivity. These results are consistent with the finding of Ueno *et al.*[43] This increase in conductivity also indicates that significantly higher power values are possible if the temperature of the cooler side was increased (*cf.* ref. 11). Thermal conductivity decreased negligibly (~4.5 %) with increasing temperature, which has important implications for the efficiency of the system (*vide infra*). The thermal conductivity of ionic liquids is known to decrease by *ca.* 3%[44] and that of water increase by *ca.* 11%[45] over the same temperature range.

Having characterised the physical properties of the electrolyte, the efficiency of heat-to-power conversion can also be calculated. The maximum theoretical efficiency (η) of

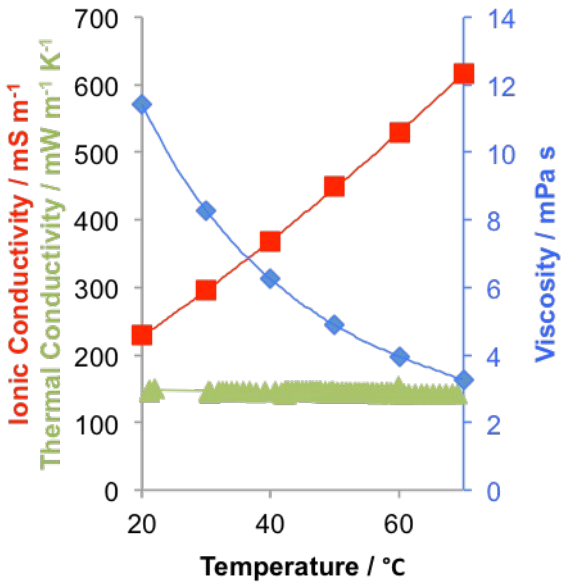

Figure 5. Temperature dependence upon the ionic conductivity (■), thermal conductivity (▲) and viscosity (◆) of 0.22 $LiNTf_2$ per G4.

a heat engine with T_c = 20 °C and T_h = 70 °C is approximately 15% (full details in supporting information).

There are several methods to calculate the efficiency, or maximum efficiency of thermoelectric systems. One simple method is to take the maximum power and divide it by the heat flow through the cell[12], using Equation 3

$$\eta = P_{max} \div \frac{A\,\lambda\,\Delta T}{d} = \frac{P_{max}\,d}{\lambda\,\Delta T} \qquad (3)$$

where η is the efficiency, P_{max} is the maximum power density, d is the distance between the electrodes, A is the cross sectional area of the cell, λ is the thermal conductivity, and ΔT is the temperature difference of the cell. For the system with clean lithium and a mole ratio of ~0.22 $LiNTf_2$ per G4, this is 0.0032%, or 0.022% of the maximum possible efficiency. These values are comparable to aqueous ferri/ferrocyanide systems employing platinum electrodes where reported efficiencies are typically between 0.001% and 0.7% of the maximum efficiency.[15] These values are significantly lower than systems with nanostructured electrodes, which can have apparent efficiencies approaching 4%.[12] This is because the P_{max} is calculated using the macro surface area (*e.g.* the electrode is treated as a planar, bulk shape) whereas the electroactive surface area for nanostructured materials can be orders of magnitude higher. Therefore the microscopic efficiency at a surface is generally the same, but nanostructured materials have significantly more surface and therefore appear to have significantly higher efficiency when considered as a whole.

The above analysis is useful but simplistic. More complicated approaches have been employed,[46] but these still lack some key points, such as heat transport by the migration of lithium ions across the cell while it is providing power. A more fundamental comparison is the 'Figure of Merit', Z_T, which depends solely on the properties of the electrolyte,[13] as defined in Equation 4:

$$Z_T = \frac{S_e^2 \sigma T}{\lambda} \quad (4)$$

where S_e is the Seebeck coefficient, as defined in equation 1, σ is the electrical or ionic conductivity of the electrolyte, or the active species of the electrolyte, T is the temperature, and λ is the thermal conductivity of the cell.

For an ideal cell, the limiting factor is the electrolyte and thus the short circuit current and open circuit potential are related to the conductance (G, given by Equation 6) of the cell, as shown in Equation 5;

$$I_{SC} = G\, V_{OC} \quad (5)$$

$$G = \frac{\sigma A}{d} \quad (6)$$

By substituting Equations 1, 2, 5 and 6 into Equation 3, the maximum theoretical efficiency of the cell is obtained, given by Equation 7, and by dividing by the maximum theoretical efficiency (Equation S1), you obtain the efficiency relative to the maximum efficiency, given by Equation 8.

$$\eta_{max} = \frac{S_e^2\, \sigma \Delta T}{4\, \lambda} = \frac{ZT_h \Delta T}{4T_h} \quad (7)$$

$$\eta_{rel_{max}} = \frac{S_e^2\, \sigma\, T_h}{4\, \lambda} = \frac{ZT_h}{4} \quad (8)$$

which simplifies to $Z_T/4$ if the temperature difference of the cell is small.

For our best performing solution (a mole ratio of 0.22 $LiNTf_2$ per G4) the ZT value at 20 °C is 0.84×10^{-3}, and at 70 °C is 2.8×10^{-3}, or Z values of 2.9×10^{-6} and 8.1×10^{-6}, respectively. These values correspond to efficiencies relative to the maximum theoretical efficiency of approximately 0.021% and 0.070% respectively. The value at 20 °C (0.021%) is in good agreement with the efficiency estimated from direct power measurements (0.022%).

The measured ionic and thermal conductivities (*cf.* Figure 4) indicate that across the ratios, *ca.* 0.25 $Li[NTf_2]$ per G4 has the highest efficiency. An increase in temperature results in an increase in the electrical conductivity but a very small decrease in the thermal conductivity (*cf.* Figure 5). This results in an overall increase in efficiency as temperature increases. For every composition the cold electrode appears to be the limiting factor.

Increasing ionic conductivity is most likely the best avenue for improving cell performance. While the Seebeck coefficient is good, and the thermal conductivity is favourably low (*ca.* 4 times lower than that of aqueous systems), the ionic conductivity is *ca.* 200 times lower than that of aqueous 0.26 M potassium ferricyanide, 0.26 M potassium ferrocyanide and 0.8 M potassium chloride;[15] the latter system gave efficiency values between 0.08% - 0.60% at pre-treated, directly heated platinum electrodes.[15] Enhancing conductivity while maintaining the other favourable characteristics of the $Li[NTf_2]$/G4 system will result in a superior systems. Recently, Ueno *et al.* have demonstrated that even after dilution of the 1:1 $Li[NTf_2]$/G4 solvate ionic liquid with acetonitrile the glyme/lithium complex persists.[47] The ionic conductivity also increases from 160 mS m^{-1} to a maximum of *ca.* 3,000 mS m^{-1} (at 30°C).[47]

Long-term discharge of the 0.22 $Li[NTf_2]$: G4 system

In order to measure the long-term effectiveness of these systems various long-term discharge experiments were performed over a number of weeks. Figure 6(a) displays example data from a cell with 0.22 $Li[NTf_2]$ per G4, which was continuously short circuited over a period of 40 days. The short circuit current density displayed an initial minor decrease over 2 hours, followed by a significant increase over 12 hours (doubling the short circuit current density), followed by a gradual decrease over time. Periodically ceasing and resuming discharge did not recover performance, demonstrating the minor role of concentration gradients in this decrease. Some cells demonstrated initial increases in the current density, while others started off with high current densities followed by rapid decreases. These differences account for the variable

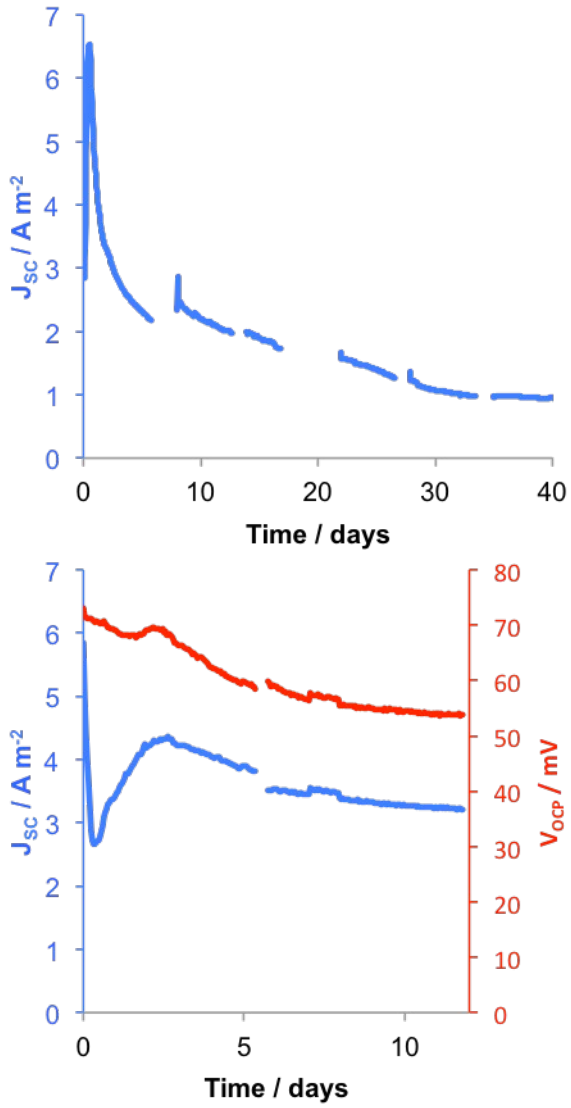

Figure 6. Short circuit current density (blue) and open circuit potential (red) of cells prepared with 0.22 $LiNTf_2$ per G4, either continually short-circuited (a) or undergoing alternating open circuit potential and short circuit measurements (b). Gaps indicate where data measurement was ceased in order to see if the cells would recover.

power densities found for cleaned Li disc electrodes in Figure 3.

After periods of extended discharge (*e.g.* 40 days) cells were opened and, as would be expected, a significant amount of lithium had migrated from the cold side to the hot side of the cell (displayed in Figure S5). A hole appeared in the cold electrode foil and, once this was depleted, the lithium ions had to diffuse from under the washer, hence accounting for the lower current density after the first 24 h. Interestingly, the lithium deposits on the hot electrode foil was extremely porous in nature, and occupied most of the volume of the cell (*cf.* Figure S5). As opposed to distinct lithium dendrites common to lithium anode batteries,[27] the material was universally porous and low density, with no evidence of short-circuiting occurring.

The precise mechanism for the dissolution of the cold anode, and growth of the hot cathode, is currently unknown. Yoshida *et al*. have demonstrated that the kinetically limiting step in a Li|1:1 Li[NTf_2]:G4|Li cell is the breaking of a single ether-Li^+ bond; likely the final bond.[32] The high Seebeck coefficient demonstrated here suggests the thermoelectrochemical (*i.e.* thermodynamic) process spans a concerted process involving more than one ether-Li^+ bond being broken.

A decreasing separation between the electrodes (due to porous lithium deposits) would be characterised by decreases in both the open circuit potential and short circuit current density, due to a smaller temperature difference. This was probed by exposing cells to a continuous temperature gradient, by alternately measuring the open circuit potential and then short current density (as opposed to continuously short circuiting). Figure 6(b) displays data for a typical cell. This much more gradual discharge recorded over 12 days is equivalent to the first 3 days of continuous short circuiting. It displays an initial drop in current followed by a period of recovery, which displays significant similarity to a typical nucleation profile. This is characterised by an initial Cottrell-type decay in current followed by an increase in current as the electrode substrate becomes more textured due to 3D, hemi-spherical growing nuclei which result in enhanced flux due to hemispherical diffusion to the textured surface.[48] This is consistent with the electrodeposition of higher surface area porous Li metal occurring at the hot cathode electrode surface.

As shown in Figure 6(b) the OCP gradually decreased as the cell was discharged, which is consistent with a smaller thermal gradient due to the enlargement of the hot electrode.

If discharging the cell results in the formation of high surface area lithium deposits, constantly alternating the temperature difference should result in high surface area electrodes at both sides. This was confirmed in a series of experiments. Figure 7 displays the results when a cell was exposed to a temperature difference (30 K; T_c = 20 °C and T_h = 50 °C) that inverted every 2 h while continually short-circuiting the cell. The short circuit current density was observed to essentially double over a period of 5 days, consistent with successive increases in the electrode surface area. The temperature difference was restricted to 30 K in order to facilitate temperature inversion, and thus accounts for the lower current density in Figure 7 relative to Figure 6. Similar trends were also observed at 50 K temperature differences. This shows that the cells can be continuously operated over periods of weeks; thermal cycling and repeated use actually improves performance over time, as opposed to lithium batteries which tend to degrade with repeated charging and discharging.[27]

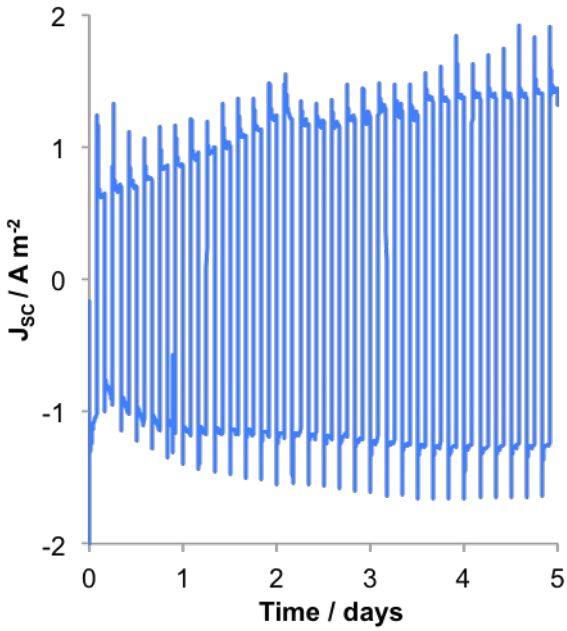

Figure 7. Short circuit current density of cell prepared with 0.22 $LiNTf_2$ per G4, continually short-circuited, with the temperature gradient alternating between 30 K and -30 K.

Conclusions

This work has demonstrated that combinations of lithium bis(trifluoromethylsulfonyl)imide (Li[NTf_2]) and tetraglyme (G4) are promising thermoelectrochemical electrolytes when combined with lithium metal electrodes. The G4 molecules complex with the lithium cations; entropy changes associated with release of the G4 molecules are the thermodynamic driving force of the thermoelectrochemical cell. This results in good Seebeck coefficients between *ca.* +0.9 and +1.4 mV K^{-1}, the colder lithium electrode dissolving and the hotter electrode growing (by electrodeposition). Optimum power was obtained from a ratio of *ca*. one Li[NTf_2] per four G4 molecules; above this ratio the electrolyte suffered from increasing viscosity, and at even high ratios a lack of un-complexed G4 molecules was also significant. The electrodeposited lithium is significantly more porous than typical lithium metal, such that repeated use of the cell results in increased electrode surface area, and thus enhanced performance. The thermal conductivity of all of the Li[NTf_2]/G4 mixtures investigated are favourably low, being on par with that of ionic liquids. However, conductivity values are also relatively low, and represent a major limiting factor in the performance and efficiency of the thermoelectrochemical cells.

Acknowledgements

The Australian Research Council (ARC DECRA DE130100770) is acknowledged for funding.

Notes and references

1. C. B. Vining, *Nature Materials*, 2009, **8**, 83-85.
2. H. Im, H. G. Moon, J. S. Lee, I. Y. Chung, T. J. Kang and Y. H. Kim, *Nano Research*, 2014, **7**, 443-452.
3. D. M. Rowe, *Thermoelectrics Handbook: Macro to Nano*, CRC Press, 2005.
4. G. S. Nolas, D. T. Morelli and T. M. Tritt, *Annual Review of Materials Science*, 1999, **29**, 89-116; B. C. Sales, D. Mandrus and R. K. Williams, *Science*, 1996, **272**, 1325-1328.
5. S. M. Kauzlarich, S. R. Brown and G. J. Snyder, *Dalton Transactions*, 2007, 2099-2107.
6. L. D. Hicks and M. S. Dresselhaus, *Physical Review B*, 1993, **47**, 727-731; R. Venkatasubramanian, E. Siivola, T. Colpitts and B. O'Quinn, *Nature*, 2001, **413**, 597-602.
7. M. S. Romano, N. Li, D. Antiohos, J. M. Razal, A. Nattestad, S. Beirne, S. Fang, Y. Chen, R. Jalili, G. G. Wallace, R. Baughman and J. Chen, *Adv Mater*, 2013, **25**, 6602-6606.
8. T. J. Abraham, D. R. MacFarlane, R. H. Baughman, N. Li, Y. Chen and J. M. Pringle, *MRS Online Proceedings Library*, 2013, **1575**.
9. T. J. Abraham, D. R. MacFarlane and J. M. Pringle, *Chemical Communications*, 2011, **47**, 6260-6262.
10. T. J. Abraham, D. R. MacFarlane and J. M. Pringle, *Energy & Environmental Science*, 2013, **6**, 2639-2645.
11. Y. Mua and T. I. Quickenden, *Journal of The Electrochemical Society*, 1996, **143**, 2558-2564.
12. R. Hu, B. A. Cola, N. Haram, J. N. Barisci, S. Lee, S. Stoughton, G. Wallace, C. Too, M. Thomas, A. Gestos, M. E. Cruz, J. P. Ferraris, A. A. Zakhidov and R. H. Baughman, *Nano Lett*, 2010, **10**, 838-846.
13. M. S. Romano, J. M. Razal, D. Antiohos, G. Wallace and J. Chen, *Journal of Nanoscience and Nanotechnology*, 2015, **15**, 1-14.
14. M. Almaimani, J. J. Black and L. Aldous, *Electrochemistry Communications*, 2016, **Submitted**.
15. T. I. Quickenden and Y. Mua, *Journal of The Electrochemical Society*, 1995, **142**, 3985-3994.
16. A. Gunawan, C. H. Lin, D. A. Buttry, V. Mujica, R. A. Taylor, R. S. Prasher and P. E. Phelan, *Nanoscale and Microscale Thermophysical Engineering*, 2013, **17**, 304-323.
17. A. Gunawan, H. Li, C. H. Lin, D. A. Buttry, V. Mujica, R. A. Taylor, R. S. Prasher and P. E. Phelan, *International Journal of Heat and Mass Transfer*, 2014, **78**, 423-434.
18. M. Bonetti, S. Nakamae, M. Roger and P. Guenoun, *Journal of Chemical Physics*, 2011, **134**, 114513.
19. E. H. B. Anari, M. Romano, W. X. Teh, J. J. Black, E. Jiang, J. Chen, T. Q. To, J. Panchompoo and L. Aldous, *Chemical Communications*, 2016, **52**, 745-748.
20. M. A. Lazar, D. Al-Masri, D. R. MacFarlane and J. M. Pringle, *Physical chemistry chemical physics*, 2015, **18**, 1404-1410.
21. N. S. Hudak and G. G. Amatucci, *Journal of The Electrochemical Society*, 2011, **158**, A572-A572.
22. S. Tang and H. Zhao, *RSC Advances*, 2014, **4**, 11251-11251.
23. T. Mandai, K. Yoshida, K. Ueno, K. Dokko and M. Watanabe, *Physical chemistry chemical physics*, 2014, **16**, 8761-8772.
24. K. Ueno, K. Yoshida, M. Tsuchiya, N. Tachikawa, K. Dokko and M. Watanabe, *The Journal of Physical Chemistry B*, 2012, **116**, 11323-11331.
25. K. Yoshida, M. Nakamura, Y. Kazue, N. Tachikawa, S. Tsuzuki, S. Seki, K. Dokko and M. Watanabe, *Journal of the American Chemical Society*, 2011, **133**, 13121-13129.
26. M. Balaish, A. Kraytsberg and Y. Ein-Eli, *Physical chemistry chemical physics*, 2014, **16**, 2801-2801; J. Scheers, S. Fantini and P. Johansson, *Journal of Power Sources*, 2014, **255**, 204-218; Y. Gambe, Y. Sun and I. Honma, *Scientific reports*, 2015, **5**, 8869-8869; K. Takechi, Y. Kato and Y. Hase, *Adv Mater*, 2015, **27**, 2501–2506; R. Tatara, N. Tachikawa, H.-M. Kwon, K. Ueno, K. Dokko and M. Watanabe, *Chemistry Letters*, 2013, **42**, 1053-1055.
27. K. Xu, *Chemical Reviews*, 2004, **104**, 4303-4417.
28. H. Moon, R. Tatara, T. Mandai, K. Ueno, K. Yoshida, N. Tachikawa, T. Yasuda, K. Dokko and M. Watanabe, *The Journal of Physical Chemistry C*, 2014, **118**, 20246-20246; B. McLean, H. Li, R. Stefanovic, R. J. Wood, G. B. Webber, K. Ueno, M. Watanabe, G. G. Warr, A. Page and R. Atkin, *Physical chemistry chemical physics*, 2015, **17**, 325-333; G. Vanhoutte, N. R. Brooks, S. Schaltin, B. Opperdoes, L. Van Meervelt, J.-P. Locquet, P. M. Vereecken, J. Fransaer and K. Binnemans, *The Journal of Physical Chemistry C*, 2014, **118**, 20152–20162.
29. C. Zhang, K. Ueno, A. Yamazaki, K. Yoshida, H. Moon, T. Mandai, Y. Umebayashi, K. Dokko and M. Watanabe, *The Journal of Physical Chemistry B*, 2014, **118**, 5144-5153.
30. T. Murphy, S. Callear, K. Shimizu, J. N. Canongia Lopes, Y. Nageshwar, M. Watanabe, T. Darwish, G. G. Warr and R. Atkin, *Physical chemistry chemical physics*, 2016, **in press**, DOI: 10.1039/C1036CP00176A.
31. K. Shimizu, A. A. Freitas, R. Atkin, G. G. Warr, P. A. FitzGerald, H. Doi, S. Saito, K. Ueno, Y. Umebayashi, M. Watanabe and J. N. Canongia Lopes, *Physical chemistry chemical physics*, 2015, **17**, 22321-22335.
32. K. Yoshida, M. Tsuchiya, N. Tachikawa, K. Dokko and M. Watanabe, *The Journal of Physical Chemistry C*, 2011, **115**, 18384-18394.
33. S. Terada, T. Mandai, R. Nozawa, K. Yoshida, K. Ueno, S. Tsuzuki, K. Dokko and M. Watanabe, *Physical chemistry chemical physics*, 2014, **16**, 11737-11746.
34. G. H. Lane, A. S. Best, D. R. MacFarlane, A. F. Hollenkamp and M. Forsyth, *Journal of The Electrochemical Society*, 2010, **157**, A876.
35. H. S. Carslaw and J. C. Jaeger, *Conduction of heat in solids*, Clarendon Press, Oxford, 1959.
36. G. J. Kluitenberg, B. S. Das and K. L. Bristow, *Soil Science Society of America Journal*, 1995, **59**, 719-726.

37. H. A. H. Alzahrani, J. J. Black, D. Goonetilleke, J. Panchompoo and L. Aldous, *Electrochemistry Communications*, 2015, **58**, 76-79.
38. K. M. Bae, H. D. Yang, L. T. Tufa and T. J. Kang, *International Journal of Precision Engineering and Manufacturing*, 2015, **16**, 1245-1250.
39. W. A. Henderson, N. R. Brooks, W. W. Brennessel and V. G. Young, *Chemistry of Materials*, 2003, **15**, 4679-4684.
40. Y. Marcus, *Pure and Applied Chemistry*, 1985, **57**, 1129-1132.
41. C. A. Paddon, S. E. Ward Jones, F. L. Bhatti, T. J. Donohoe and R. G. Compton, *Journal of Physical Organic Chemistry*, 2007, **20**, 677-677.
42. M. J. Schmid, K. R. Bickel, P. Novák and R. Schuster, *Angewandte Chemie - International Edition*, 2013, **52**, 13233-13237.
43. K. Ueno, K. Yoshida, M. Tsuchiya, N. Tachikawa, K. Dokko and M. Watanabe, *The Journal of Physical Chemistry B*, 2012, **116**, 11323-11331.
44. R. Ge, C. Hardacre, P. Nancarrow and D. W. Rooney, *Journal of Chemical & Engineering Data*, 2007, **52**, 1819-1823.
45. M. L. V. Ramires, C. A. Nieto de Castro, Y. Nagasaka, A. Nagashima, M. J. Assael and W. A. Wakeham, *Journal of Physical and Chemical Reference Data*, 1995, **24**, 1377-1381.
46. G. J. Snyder and T. S. Ursell, *Physical Review Letters*, 2003, **91**, 148301; H. S. Kim, W. Liu, G. Chen, C.-W. Chu and Z. Ren, *Proceedings of the National Academy of Sciences*, 2015, **112**, 8205-8210.
47. K. Ueno, J. Murai, K. Ikeda, S. Tsuzuki, M. Tsuchiya, R. Tatara, T. Mandai, Y. Umebayashi, K. Dokko and M. Watanabe, *The Journal of Physical Chemistry C*, 2016, **In press**, DOI: 10.1021/acs.jpcc.1025b11642.
48. D. Pletcher, *A first course in electrode processes*, The Electrochemical Consultancy, Hampshire, 1991.